Molecular quantum wake-induced pulse shaping and extension of femtosecond air filaments

S. Varma, Y.-H. Chen, J. P. Palastro, A. B. Fallahkair, E. W. Rosenthal, T. Antonsen, and H. M. Milchberg
Institute for Research in Electronics and Applied Physics, University of Maryland, College Park, Maryland 20742, USA
(Received 5 March 2012; published 28 August 2012)

Two-pulse excitation of a molecular quantum wake in air during filamentary propagation is shown to controllably shape an intense femtosecond probe pulse and to significantly extend the filament compared to single-pulse excitation. The effect is sensitive to pump-probe delay on a ∼10-fs time scale.

DOI: 10.1103/PhysRevA.86.023850 PACS number(s): 42.65.Re, 42.65.Jx, 52.38.Hb, 37.10.Vz

I. INTRODUCTION

The filamentation of femtosecond laser pulses in solids, liquids, and gases, accompanied by plasma generation, is rich in nonlinear physics and applications [1]. The recent experimental demonstration that quantum molecular rotational revivals in the atmosphere [2] can have a dominant effect on filament propagation has accompanied a resurgence of interest in filamentation and applications [3]. The rotational revivals propagate behind a filamenting pump pulse like a wake, and this wake can steer, trap, or destroy an intense injected probe pulse. The molecular rotational response is sufficiently fast that it dominates the propagation of single ∼100-fs pulses filamenting in the atmosphere [4,5].

In this paper, we demonstrate that a molecular quantum wake can shape a filamenting probe pulse while significantly extending the nonlinear propagation distance and plasma generation. It does so by disrupting the usual interplay between nonlinear focusing and plasma defocusing responsible for extended filament propagation. In a single-pulse filament, the radially confined high intensity region (typically <100 μm in diameter) is not really akin to the intensity confinement in a glass [6] or plasma [7] optical fiber where there is little transverse energy exchange with zones outside the confinement region. In a typical single-pulse filament, the high intensity region is sustained by simultaneous incoming and outgoing energy exchange with a wider co-propagating "reservoir" [8] whose transverse extent is roughly defined by the spatial envelope of the original beam. Here, we show that, by applying an intense probe pulse to the co-propagating rotational wake induced by the pump pulse, the wake is shaped and is enhanced so as to self-consistently support an enhanced filament in which quantum molecular lensing dominates both Kerr focusing and plasma defocusing. Remarkably, the wake shaping and filament extension are sensitive to pump-probe delay on a 10-fs time scale. Theory and simulations agree well with experiments and provide significant insight. Prior work by other groups explored the cross-phase modulation and guiding of weak probe pulses in molecular alignment revivals generated in short nitrogen filaments [9]. In addition, simulations have shown filament extension by probe pulses sampling prefixed molecular alignment produced by a nonfilamenting pump [10]. Extension of a probe filament in the wake of a filamenting pump has been qualitatively inferred from plasma fluorescence measurements [11]. However, pulse shaping and filament plasma extension have never been directly measured, nor has a self-consistent two-pulse filamentation simulation been performed.

II. DIRECT MEASUREMENT OF FILAMENT PLASMA DENSITY AND FILAMENTING PULSE ELECTRIC FIELD

Our experiment measures both the electron-density profile produced in the probe pulse-enhanced filament and the envelope and phase of the probe pulse exiting the filament (using the spectral phase interferometric direct electric-field reconstruction (SPIDER) technique [12]). Figure 1(a) shows the experimental setup. Orthogonally polarized collinear pulses (pump and probe) pass through a 3.1-m focal length lens, immediately followed by a 5.5-mm diameter aperture (not shown). The probe is delayed in 13-fs steps by a computer-controlled stepper motor. The orthogonal polarization allows later separation of the probe pulse for the SPIDER measurements. For the electron-density diagnostic, a probe beam split from the main beam counterpropagates across the filament axis at 0.75° and enters a folded wave-front imaging interferometer mounted on a carriage with 2 m of translation along the filament axis. The small crossing angle enhances the sensitivity to the low electron density of filaments (typically on the order of $\sim 10^{16}$ cm^{-3} [4]) with the price paid being a reduced axial resolution of ∼5 mm, which is of little concern for our meter-scale filaments.

Our technique allows measurement of plasma density as low as $\sim 5 \times 10^{14}$ cm^{-3} with a transverse resolution of 5 μm. Transverse density profiles, averaged from 200 shots at each position, were measured every 2 cm along the filament and were extracted using standard phase extraction techniques [13]. For all measurements, the pump energy and pulse width were $\varepsilon_{\text{pump}} = 1.5$ mJ and $\tau = 80$ fs, which formed extended single filaments as expected at $\sim 1.9 P_{\text{cr}}$ where the critical power for self-focusing was measured to be $P_{\text{cr}} \sim 10$ GW at this pulse width [2]. The probe pulse energy $\varepsilon_{\text{probe}}$ was varied in the range of 1.0–2.5 mJ with a pulse width of 90 fs. All parameters were measured after the lens. We ensured single transverse filament propagation in the two-pulse case by monitoring the axial and radial electron-density profiles as well as the white-light spot in the filament far field.

The effect of delaying the injection of a 1.85-mJ probe pulse into the filament formed by the pump is shown in the electron-density profile measurements of Fig. 1(b). The range of delays chosen is near the zero crossing of the first rotational revival of air [as seen by the probe at a 8.341-ps delay from the peak of the pump; Fig. 4(a) shows the simulated delays] formed from the full revival of N_2 and the $\frac{3}{4}$ revival of O_2, which have a sum effect on the air refractive index [2]. With the pump alone, filament formation and plasma generation occur well

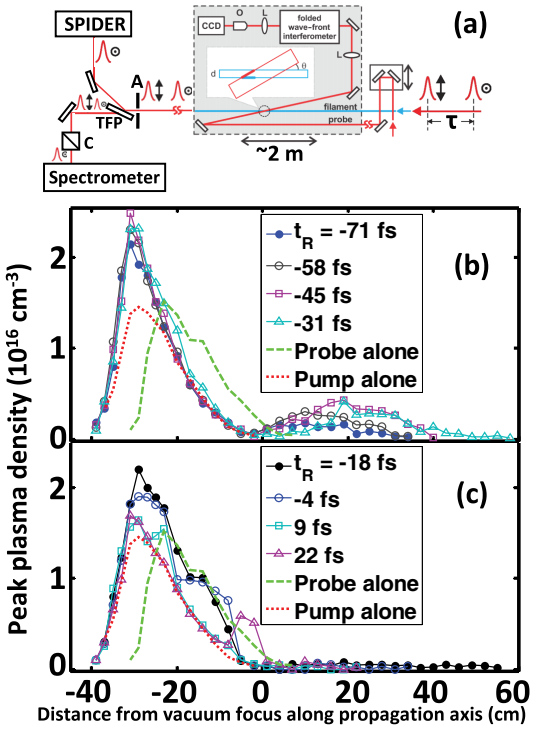

FIG. 1. (Color online) (a) Experimental setup showing the interferometer for measuring electron-density profiles and SPIDER for measuring the envelope and phase of the probe pulse. (b) Electron density at the center of the filament core vs distance (in cm) relative to the laser vacuum focus. Probe delays are all in advance of the air revival zero crossing at 8.341 ps. (c) Same as (b), except probe delays are closer to and beyond the zero crossing.

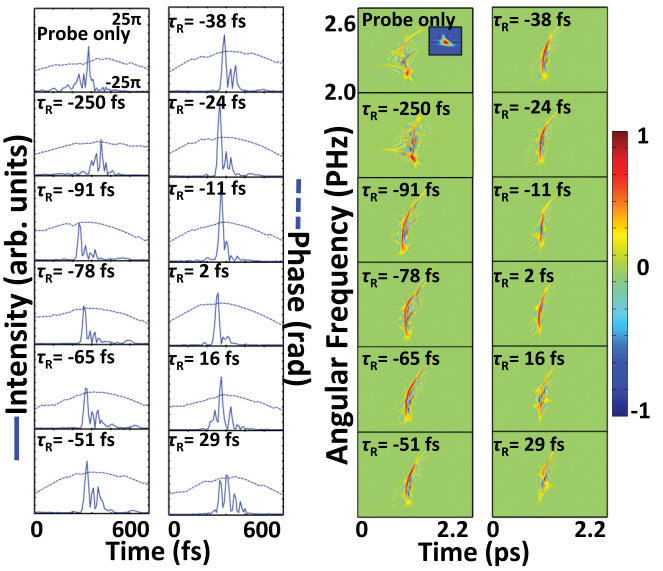

FIG. 2. (Color online) Left side: envelope $I(t)$ and phase $\Phi(t)$ plots of the probe pulse exiting the two-pulse filament. The shortest pulse, with 21-fs FWHM, occurs in the range of -11 fs $< t_R < 2$ fs. For all probe delays, $\partial^2\Phi/\partial t^2 < 0$ throughout the pulse envelope, indicating a dominant redshift to blueshift. Right side: Wigner plots corresponding to the plots on the left. The Wigner plot for the prefilamenting probe alone is shown highlighted in the upper left panel.

before the vacuum focus ($z = 0$ on the axial scale) with a peak density of $\sim 1.5 \times 10^{16}$ cm^{-3} and an axial extent of $\sim$25 cm. The probe-alone filament, with a similar shape, is displaced forward by $\sim$10 cm owing to the slightly more diverging probe beam. The general form of the pump plus probe filaments is a $\sim$70% enhanced first peak ($\sim$100% at $\varepsilon_{\text{probe}} = 2.5$ mJ) followed by a long electron density hump (peak $\sim 0.5 \times 10^{16}$ cm^{-3}) extending to $z \sim 40$ cm. The overall filament length is approximately tripled at the optimum probe delay of $t_R \sim -30$ fs with respect to the zero crossing of the air revival. Extended filaments, which show a remarkably fine sensitivity to probe delay on $\sim$10-fs time scale, appear over an $\sim$50-fs range of -70 fs $< t_R < -20$ fs. For delays $t_R > -20$ fs, the electron density in the extended part of the filament abruptly drops to close to our threshold sensitivity level. Figure 1(c) shows the sequence of electron-density profiles for these longer delays where there is little extended density enhancement, but the two-pulse electron-density envelope now encompasses both pump- and probe-alone filaments. This extension of the initial density hump for positive t_R is reproduced by the simulations as seen below. The result of the full probe energy scan (1–2.5 mJ) showed similar behavior: two peaks with enhanced density for mainly negative t_R, and for positive t_R, no significant density enhancement but a wider two-pulse peak encompassing the pump- and probe-alone filaments. In both cases, little overall density increase occurred from 1.8 to 2.5 mJ.

The effect on an intense probe pulse's envelope and phase from propagation in the pump-induced molecular wake was measured by SPIDER [12]. The goal was to extract this information from the central high intensity filament where the biggest amplitude rotational wake was concentrated. The pump and probe were orthogonally polarized (see Fig. 1), allowing the probe to be filtered off by reflection from an ultrabroadband thin-film polarizer. The beam was passed through a 1.3-mm diameter aperture centered on the central supercontinuum spot 2 m after the end of the filament, defined as the location beyond which the electron density was below our measurement threshold. It then propagated another 3.28 m to the nonlinear crystal in the SPIDER. It was found that the extracted pulse envelope and phase converged well for apertures of diameter $d < 1.5$ mm; above 2 mm, SPIDER results were aperture dependent owing to beam nonuniformities and interference effects.

The probe field in the spectral domain $|\tilde{E}(\omega)|e^{i\phi(\omega)}$ was determined as follows. For each pump-probe time delay, 200 SPIDER spectral interferograms (200 laser shots) were taken. The spectral phase $\phi(\omega)$ was extracted from the average of all of the interferograms, and the spectral amplitude $|\tilde{E}(\omega)|$ was taken from an auxiliary spectrometer. The time-dependent field $|E(t)|e^{i\Phi(t)}$ is the Fourier transform of $|\tilde{E}(\omega)|e^{i\phi(\omega)}$. Note that $\phi(\omega)$ was corrected for the air group-velocity dispersion of $\beta = 22$ fs^2/m [14] experienced in propagation from the end of the filament to the SPIDER. This amounted to a correction of less than 10 rad in the spectral wings of the pulse.

Figure 2 shows intensity vs time plots $I(t) \propto |E(t)|^2$ and corresponding Wigner plots for a sequence of pump-

probe delays before and during the air quantum revival near 8 ps. The Wigner distribution [15] is a useful time- and frequency-domain representation of an ultrashort pulse that explicitly displays chirp. The temporal phase $\Phi(t)$ is also shown superimposed as a dashed line on $I(t)$. Here, the probe energy is 2.5 mJ. Note that the "probe only" pulse breaks up into multiple spikes in both time and frequency as is consistent with filamentary self-focusing of different time slices in the pulse [8] and interference of spectral components nonlinearly generated by self-phase modulation. With the pump on and the probe delayed by 8.25 ps ($t_R = -250$ fs) well before the air revival, it is similarly broken up. As the delay moves inside the air revival, the pulse develops a dominant leading spike followed by much smaller wings. For -30 fs $< t_R <$ 16 fs, a ~50 fs interval, $I(t)$ shows an especially dominant single peak with reduced temporal wings. In this interval, the Wigner traces become smoothly arcing and compact with a strong redshift to blueshift from the front to the back of the pulse. The leading redshift is attributable to the air molecular alignment induced in the pulse leading edge [2,4], and the blueshift is from plasma generation. Beyond this interval, the pulse begins to break up again in time and frequency. We note that the pump-probe delay interval, corresponding to the axially extended filaments of Fig. 1(b), sits about ~40 fs earlier than the interval associated with pulse shortening shown in Fig. 2. In fact, pulse shortening appears to favor delays in the range of Fig. 1(c), and this is explained by our propagation simulations. Two other probe energies were used, 1.0 and 1.6 mJ, with similar results.

III. NONPERTURBATIVE SIMULATION OF TWO-PULSE ALIGNMENT

The sensitivity of filament enhancement and pulse shaping to pump-probe delay is explained by the two-pulse excitation of molecular quantum wave packets in air: The probe pulse's strong modification of the pump filament-induced molecular alignment depends finely on delay. We have modeled the two-pulse-induced ensemble average molecular rotational response $\Delta n_{\rm rot}$ using nonperturbative density-matrix simulations of a gas of 80% N_2 and 20% O_2 molecules illuminated by femtosecond optical pulses. We also compute the instantaneous electronic response $\Delta n_{\rm elec} = n_2 I$ using, for air, $n_2/n_{2,\rm long} = 0.2$ as recently determined [5], where $n_{2,\rm long} I$ is the long pulse (adiabatic) rotational response. The rotational effect dominates the total response. Figure 3 shows $\Delta n = \Delta n_{\rm rot} + \Delta n_{\rm elec}$ in air as seen by the probe pulse, produced by a 100-fs 2×10^{13}-W/cm^2 pump pulse (typical clamping intensity in a filament core [1]) followed by a similar, but variably delayed and perpendicularly polarized, intense probe. It is seen that, by varying the probe delay in a <150-fs window around the positive index peak, one obtains a factor of ~2 variation in the index change it experiences. This is due to the strong delay dependence of the two-pulse-induced molecular alignment. As will be seen, simulations, which are consistent with experiments, show a much finer delay sensitivity owing to the cumulative effect this index change has on the pulse envelope and profile from long-scale-length propagation. Figure 3 also provides a qualitative explanation for the probe-enhanced electron density of Fig. 1(b): The

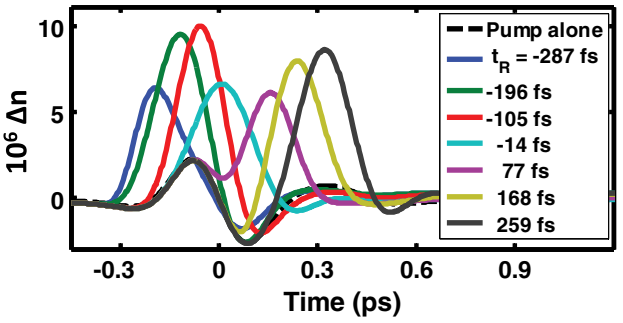

FIG. 3. (Color online) Density-matrix simulation of the self-consistent refractive index change experienced by a variably delayed 2×10^{13} W/cm^2 100-fs probe pulse perpendicularly polarized with respect to a similar pump pulse. The probe delays t_R are relative to the zero crossing of the pump-induced air rotational revival near 8.3 ps, shown as the dashed curve.

focusing promoted by the enhanced molecular response $\Delta n \sim 10^{-5}$ is offset by a peak plasma index $\Delta n_{pl} \sim -N_e^{\rm peak}/2N_{\rm cr}$, giving $N_e^{\rm peak} \sim 3 \times 10^{16}$cm^{-3}. That the filament length is also strongly affected is unsurprising given the large enhancement in optical nonlinearity promoted by the additional alignment. However, both the filament length dynamics and the probe pulse evolution are two-dimensional (2D) effects best explained by propagation simulations, and we now present those.

IV. SELF-CONSISTENT 2D PROPAGATION SIMULATION

Full details of the simulations are described in Ref. [16]. The pump and probe pulses are evolved self-consistently via the extended paraxial wave equation $[\frac{2}{c}\frac{\partial}{\partial z}(i\omega_0 - \frac{\partial}{\partial \tau}) - \beta_2 \frac{\partial^2}{\partial \tau^2} + \nabla_\perp^2]a = [\frac{4\pi q^2 n_e}{mc^2} - k_0^2(\delta\varepsilon_s + \delta\varepsilon_r)]a$, where $a(r,z,\tau)$ is the complex envelope of either the pump or the probe laser field, $k_0 = \omega_0/c$ is the central wave number of the initial pulse, r is the transverse coordinate, z is the propagation distance, $\tau = t - z/v_g$ is time local to the pulse frame moving at group velocity v_g, $\beta_2 = k_0(d^2k/d\omega^2)_{\omega=\omega_0}$ is the group-velocity dispersion of air, $q = -e$ is the electron charge, and n_e is the electron density generated by laser ionization. Plasma formation by laser-driven ionization is modeled using rates from Ref. [17].

The self-modification of the refractive index due to the instantaneous and delayed (rotational) responses is represented by $\delta\varepsilon_s = \delta\varepsilon_i + \delta\varepsilon_d$, where the instantaneous electronic response is $\delta\varepsilon_i = 2n_2 I(r,\tau)(I \propto |a|^2)$ and the delayed rotational response $\delta\varepsilon_d$ is given by $[\frac{d^2}{d\tau^2} + 2\gamma_d \frac{d}{d\tau} + \omega_d^2]\delta\varepsilon_d = 2\omega_d^2 n_{20} I(r,\tau)$, where γ_d, ω_d, and n_{20} are determined by fits to our femtosecond time-resolved measurements of the air rotational response [4,5]. The term $\delta\varepsilon_r$ in the wave equation accounts for the index modification encountered by the probe due to revivals in the molecular alignment. This term is zero for the pump pulse. To determine the index modification set up by the pump pulse after one rotational revival period, we solve $[\frac{d^2}{d\tau^2} \pm 2\gamma_d \frac{d}{d\tau} + \omega_d^2]\delta\varepsilon_{r,\pm} = \pm 2\omega_d^2 n_2 I(r,\tau - T)$, where $\delta\varepsilon_r = \delta\varepsilon_{r,+} + \delta\varepsilon_{r,-}$, T is the full recurrence period, and I is the intensity of the pump. Integrating both forward $(+)$ and backward $(-)$ in τ ensures the response has the appropriate

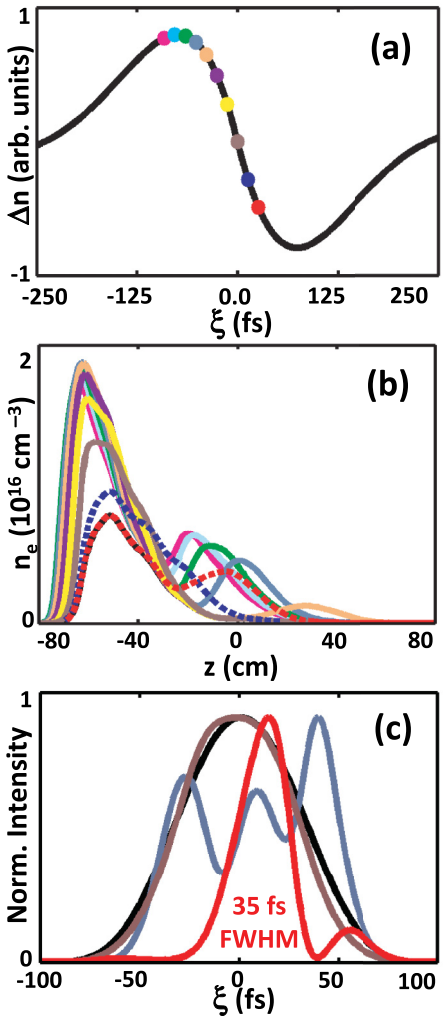

FIG. 4. (Color online) (a) Pump-induced index variation at first air revival as seen by the probe. The colored dots denote probe delays t_R relative to the revival zero crossing. From left to right, $t_R = -91$, -78, -65, -52, -39, -26, -13, 0, 13, and 26 fs. Solid black curve: pump-alone and probe-alone curves are the same and sit under the first hump of the red-dashed curve. (b) Two-pulse axial electron-density profiles. Dashed curves are for $t_R > 0$. The ∼10-fs probe delay sensitivity of Fig. 1 is well reproduced. Solid black curve: pump-alone and probe-alone curves are the same and sit under the first hump of the red-dashed curve. (c) Probe pulse envelopes for delays before (grey) and after (red) the revival zero crossing. The shortest compressed pulse is 35 fs FWHM. The black curve is the initial probe envelope, and the brown curve is for $t_R \sim 0$. Peak signals are normalized to unity.

antisymmetry about the recurrence zero crossing observed in our density-matrix simulations.

Figure 4 shows the simulated on-axis electron-density profiles for a sequence of pump-probe delays relative to the revival zero crossing. The absolute densities calculated are in reasonable agreement with experiment. The density profiles show three types of behavior. For delays near the peak of the pump-induced alignment revival, the probe experiences the strongest focusing phase of the alignment, and it focuses earlier than in the absence of the pump. It generates additional plasma, refracts, and then refocuses downstream in the combined pump-probe index, creating the second electron-density hump. The range of delays producing an extended filament in this manner is ∼50 fs, consistent with the experimental plots of Fig. 1(b). The ∼10-fs sensitivity with respect to probe delay of the second hump generation matches the experimental results of Figs. 1(b) and 1(c). With delays approaching the zero crossing, the probe pulse experiences a smaller self-augmented focusing effect. It focuses slightly earlier than in the absence of the pump, enhances the existing plasma density, and refracts with the probe-augmented alignment insufficient to cause refocusing and an additional plasma hump. This is seen in the evolution of Figs. 1(b) to 1(c) where the second hump disappears between -31 and -18 fs. Finally, for delays $t_R > 0$, the probe encounters the defocusing phase of the pump's recurrence and focuses further downstream than the pump, generating an additional plasma hump (dashed curves). The range of delays in this regime, yielding a slightly extended filament, is ∼15 fs. For corresponding delays in the experiment, Fig. 1(c), the two-pulse filament was extremely unstable with large shot-to-shot variations in the electron density, averaging to low levels in the filament extension region. This is consistent with the very narrow delay window in the simulations. However, in this $t_R > 0$ delay range, the two-pulse filament encompasses both the pump- and the probe-alone filaments as observed in the experiment. In Fig. 4(c), the probe pulse envelope is shown averaged over the core of the filament ($r < 70$ μm) for delay times before and after the zero crossing. Also shown is the initial pulse shape. The core intensity acquires a temporal structure due to the time-slice-dependent focusing during filamentary propagation. The $t_R = 26$-fs delay probe pulse (red curve) initially sits in the defocusing phase of the pump's recurrence and focuses less strongly and downstream from the pump. Due to the weaker focusing and lower intensity, plasma is generated later in the pulse. The pulse appears to shorten because the front is refracted by the pump recurrence, the middle is self-focused, and the trailing portion is refracted by plasma. In contrast, the $t_R = -52$-fs delay pulse (gray curve) experiences focusing, refraction, and refocusing throughout its duration, resulting in an irregular time structure. We note that this structure applies to the core intensity. The time-dependent power, integrated over all radii, differs little from the initial pulse envelope. Although the exact delays and minimum pulse width do not match, the result is in qualitative agreement with the experimental results of Fig. 2: For large negative t_R, the pulse structure is multispiked. Only approaching the zero crossing and slightly beyond does one see a clean single pulse.

V. CONCLUSION

To summarize, we have shown that, with ∼10-fs sensitivity, we can control both the time structure of an intense filamenting pulse as well as the magnitude and spatial extent of the electron density generated during its propagation. Control is achieved by fine adjustment of the intense probe pulse delay with respect to the pump-induced first quantum rotational revival in air, contributed partially by N_2 and O_2. The probe-boosted molecular alignment results in a significantly larger nonlinearity and, therefore, enhanced filamentary propagation of the probe pulse. We note that although the dynamics are

complex and complete physical insight could only be obtained through propagation simulations, the effects are finely controllable and reproducible. This experiment constitutes a detailed demonstration of the effects and underlying physics of nonlinearity control in high intensity laser beam propagation.

ACKNOWLEDGMENTS

This research was supported by the Office of Naval Research, the National Science Foundation, and the US Department of Energy.

[1] A. Couairon and A. Mysyrowicz, Phys. Rep. **441**, 47 (2007).
[2] S. Varma, Y.-H. Chen, and H. M. Milchberg, Phys. Rev. Lett. **101**, 205001 (2008).
[3] M. Durand, Y. Liu, A. Houard, and A. Mysyrowicz, Opt. Lett. **35**, 1710 (2010); H. Cai, J. Wu, A. Couairon, and H. Zeng, *ibid.* **34**, 827 (2009).
[4] Y.-H. Chen, S. Varma, T. M. Antonsen, and H. M. Milchberg, Phys. Rev. Lett. **105**, 215005 (2010).
[5] J. K. Wahlstrand, Y.-H. Cheng, and H. M. Milchberg, Phys. Rev. A **85**, 043820 (2012).
[6] G. P. Agrawal, *Fiber-Optic Communication Systems*, edited by K. Chang, Wiley Series in Microwave and Optical Engineering, 3rd ed. (Wiley, Hoboken, NJ, 2002).
[7] T. R. Clark and H. M. Milchberg, Phys. Rev. E **61**, 1954 (2000); C. G. Durfee, J. Lynch, and H. M. Milchberg, *ibid.* **51**, 2368 (1995).
[8] M. Mlejnek, E. M. Wright, and J. V. Moloney, Opt. Lett. **23**, 382 (1998).
[9] F. Calegari, C. Vozzi, S. Gasilov, E. Bendetti, G. Sansone, M. Nisoli, S. De Silverstri, and S. Stagira, Phys. Rev. Lett. **100**, 123006 (2008).
[10] J. Wu, H. Cai, H. Zeng, and A. Couairon, Opt. Lett. **33**, 2593 (2008); J. Wu, H. Cai, Y. Peng, Y. Tong, A. Couairon, and H. Zeng, Laser Phys. **19**, 1759 (2009).
[11] H. Cai, J. Wu, H. Li, X. Bai, and H. Zeng, Opt. Express **17**, 21060 (2009).
[12] C. Iaconis and I. A. Walmsley, Opt. Lett. **23**, 792 (1998).
[13] Y.-H. Chen *et al.*, Opt. Express **15**, 11341 (2007); **15**, 7458 (2007).
[14] P. Sprangle, J. R. Penano, and B. Hafizi, Phys. Rev. E **66**, 046418 (2002).
[15] D. D. Marcenac and J. E. Carroll, Opt. Lett. **18**, 1435 (1993).
[16] J. P. Palastro, T. M. Antonsen, Jr., S. Varma, Y.-H. Chen, and H. M. Milchberg, Phys. Rev. A **85**, 043843 (2012).
[17] A. Talebpour, J. Yang, and S. L. Chin, Opt. Commun. **163**, 29 (1999).